Journal of Loss Prevention in the Process Industries 34 (2015) 209–217

Contents lists available at ScienceDirect

Journal of Loss Prevention in the Process Industries

journal homepage: www.elsevier.com/locate/jlp

Numerical study of dynamic response and failure analysis of spherical storage tanks under external blast loading

B.Y. Zhang [a, b], H.H. Li [a, b], W. Wang [a, b, *]

[a] Key Lab of Structures Dynamic Behavior and Control (Harbin Institute of Technology), Ministry of Education, Heilongjiang, Harbin, 150090, China
[b] School of Civil Engineering, Harbin Institute of Technology, Harbin, 150090, China

ARTICLE INFO

Article history:
Received 17 June 2014
Received in revised form
25 November 2014
Accepted 15 February 2015
Available online 26 February 2015

Keywords:
Spherical storage tank
TNT equivalent method
Blast impact
Dynamic response
Failure analysis

ABSTRACT

The performance of energy infrastructures under extreme loading conditions, especially for blast and impact conditions, is of great importance despite the low probability for such events to occur. Due to catastrophic consequences of structural failure, it is crucial to improve the resistance of energy infrastructures against the impact of blasts. A TNT equivalent method is used to simulate a petroleum gas vapor cloud explosion when analyzing the dynamic responses of a spherical tank under external blast loads. The pressure distribution on the surface of a 1000 m^3 spherical storage tank is investigated. The dynamic responses of the tank, such as the distribution of effective stress, structural displacement, failure mode and energy distribution under the blast loads are studied and the simulation results reveal that the reflected pressure on the spherical tank decreases gradually from the equator to the poles of the sphere. However, the effects of the shock wave reflection are not so evident on the pillars. The structural damage of the tank subjected to blast loads included partial pillar failure from bending deformation and significant stress concentration, which can be observed in the joint between the pillar and the bottom of the spherical shell. The main reason for the remarkable deformation and structural damage is because of the initial internal energy that the tank obtained from the blast shock wave. The liquid in the tank absorbs the energy of impact loads and reduces the response at the initial stage of damage after the impact of the blast.

1. Introduction

With the expanding scopes of storage of petroleum products, the possibility of accidents caused by petroleum combustible gas explosions also increases. During the past several years, a series of oil tank fires and explosion accidents caused great financial loss and casualties (Persson and Lönnermark, 2004; Abbasi and Abbasi, 2007; Chang and Lin, 2006). Most of the explosions were triggered by the detonation of a vapor cloud, which was initiated by the petroleum products themselves (Lees, 1996; Lieb, 2002). Once a combustible gas explosion occurs in petroleum facilities, chemical plants or storage areas, it may not only cause serious damage to a single oil tank, but also can lead to a chain reaction of explosions and trigger a secondary disaster. Therefore, the investigation on the failure mechanism and dynamic response of oil storage tanks subjected to combustible gas explosions is important and necessary.

Storage tanks can be cylindrical and spherical in shape. Spherical storage tanks primarily consist of the lower support structures and the spherical shell structures, which sit on support structures. Specifically, the shape of the shells can be spherical, elliptical, and teardrop-shaped, among which spherical tanks are the most widely used because for the same volume and thickness, spherical tanks use the minimum amount of steel and cover a minimum area.

During the past five decades, many researchers have investigated the dynamic behaviors (James and Raba, 1991; Sezen et al., 2008; Korkmaz et al., 2011; Moslemi and Kianoush, 2012) and failure modes (Trebuňa et al., 2009; Dogangun et al., 2009; Kim et al., 2009) of liquid-filled tanks, which were mostly cylindrical and rectangular, that had been subjected to earthquakes. The seismic responses of elevated liquid storage tanks are mainly studied because of their importance to the petrochemical industry. The effects of liquid sloshing in spherical containers have been investigated in some studies (McIver, 1989; McIver and McIver,

* Corresponding author. School of Civil Engineering, Harbin Institute of Technology, 73 Huanghe Road, Harbin, 150090, China.
E-mail addresses: zhangby@hit.edu.cn (B.Y. Zhang), wwang@hit.edu.cn (W. Wang).

http://dx.doi.org/10.1016/j.jlp.2015.02.008
0950-4230/

1993; Evans and Linton, 1993). Moreover, two recent studies presented the development of a mathematical model for quantifying the influence of the linear sloshing effects on the dynamic responses of horizontal cylindrical and spherical liquid tanks under earthquake excitation (Karamanos et al., 2006; Patkas and Karamanos, 2007). For the particular case of the dynamic behavior of elevated spherical tanks under lateral excitation, only a few works were found. For example, Drosos et al. (2005) numerically investigated the seismic response of a typical spherical liquid storage tank equipped with a nonlinear viscous bracing system.

With regards to the dynamic analysis of storage tanks under blast loads, several studies have been published using computational and experimental methods. Zhou et al. (2009) investigated the dynamic characteristics of an underground vertical tank subjected to an explosion impact. One of the key conclusions of this work was that the tank seismic check method which considered seismic loads did not apply to explosion impact loads. Lu et al. (2011a, 2011b), Lu and Wang (2012) used a combustible gas detonation device to generate a stable detonation shock wave by exploding a methane/air mixture, which was stored in the pipeline beforehand. The device was used for conducting experimental tests to study the dynamic response characteristics and failure mechanisms of large-scale storage tanks under blast impact loads.

So far, studies of dynamic response and failure analysis of spherical storage tanks under external combustible gas explosion shock waves have not been published yet. Since large scale or prototype explosion tests are very expensive, numerical simulations should be conducted in order to investigate attenuation laws and destructive effects of gas explosion shocks which will also assist the future design of experimental tests.

The present study performs numerical simulations to investigate the dynamic responses and failure modes of spherical storage tanks under external combustible gas explosions. Commercial explicit finite element software LS-DYNA (LSTC, 2007) is employed to analyze the blast resistance and energy absorption capacities of the spherical storage tanks. A TNT equivalent method is used to establish equivalent load models for petroleum gas cloud explosions. Considering the effect of material strain rate effects, the dynamic response and failure mechanism of the tanks under gas blast loads are studied to provide scientific references for the rational design of such structures in the future.

2. Finite element model

2.1. Finite element code and ALE method

The numerical simulation is carried out using the commercial software LS-DYNA, which is based on explicit numerical methods and has been widely employed to analyze the problems associated with large deformation, structure response to high velocity impact and blast load and strain rate behavior of materials. There are at least three approaches for such kind of problems: (1) Lagrangian formulation; (2) Eulerian formulation; and (3) arbitrary Lagrangian–Eulerian (ALE) formulation, which makes it possible to follow large flows of various materials without encountering numerical distortion problems often experienced in Lagrangian formulations. The Arbitrary Lagrangian–Eulerian (ALE) element formulation is a standard numerical approach for solving large deformation problems encountered in metal forming subjected to high-speed impact or blast loading. The general concept of the ALE formulation is that an arbitrary referential domain is defined for the description of motion that is different from the material (Lagrangian) and spatial (Eulerian) domains (LSTC, 2007).

3 types of elements are used herein: (1) LINK160 element: a 2-nodes beam element which is only able to carry axial loads; (2) SHELL163 element: a 4-node rectangular shell element which can carry bending moment and membrane force and both in-plane and normal loads are permitted; (3) SOLID164 element: a 8-nodes solid element used for the 3-D modeling of structures.

2.2. Numerical model for spherical tanks and explosion source

A finite element model is created for a 1000 m^3 equator tangent column spherical storage tank which consists of four parts: the spherical shell, pillars, links and connecting plates. The thickness of the shell is 45 mm. The nominal cross-section dimension of the circular pillar tubes (diameter $D \times$ thickness t) is 250 mm $\times$ 10 mm, and the dimension of the link is 48 $\times$ 6 mm. Fig. 1(a) shows the shape and the size of the spherical storage tank model. In this study, a gas containing water assumed in the spherical storage tank (Shebeko et al., 2007) was modeled using water with volume of 80% in order to simply simulate the effect of outside explosion on the tank. The distance between the explosion's center to the face of the tank was assumed to be 25 m.

2.3. Elements and meshing

Considering the actual size of the model, SHELL 163 elements are used to simulate the spherical shell, connecting plate and pillars of the spherical storage tank, and LINK 160 elements are used to represent the links. TNT, liquefied petroleum gas and air are modeled using SOLID 164 elements. Since the ALE fluid-solid coupling method cannot simultaneously consider both the inside and outside of the structure, the meshless Smooth Particle Hydrodynamics (SPH) method is used to simulate the liquid in the tank and the forces transferred from the liquid to the spherical shell can be modeled by examining the contact between them. To do so, mapping mesh is adopted. The size of shell elements and the solid elements representing TNT is 40 mm, and the size of the solid elements representing air is 100 mm.

The fluid-structure interaction is simulated by employing a coupling algorithm. The fluid is treated with an ALE fixed/mobile mesh, while the structure is treated with a Lagrangian deformable mesh. The coupling algorithm computes the coupling forces at the fluid-structure interface. These forces are added to the fluid and the structure nodal forces, which are calculated on the basis of explicit finite element analysis. Predicting the local peak pressure on the structure requires an accurate fluid-structure coupling algorithm. The ALE coupling algorithm presented in this paper uses penalty based formulation similar with the penalty contact in Lagrangian analyses.

2.4. Material models and equation of state

Explosion loading is associated with strain rate effects. The mechanical properties of steel are remarkably affected by the strain rate. Therefore, in this study, a multi-linear kinematic hardening model (MAT_PLASTIC_KINEMATIC model in LS-DYNA), which is able to take into consideration the strain rate is used to represent the responses of the Q235 steel. The initial yielding stress of the steel is 235 MPa, the elastic modulus is 206 GPa, and the Poisson ratio is 0.3. The rate-dependent plasticity model for the yielding stress of steel, proposed by Cowper and Symonds (1957) is given by:

$$\sigma_{dy} = \left[1 + \left(\frac{\dot{\varepsilon}^{pl}}{\gamma}\right)^{m}\right]\sigma_y \tag{1}$$

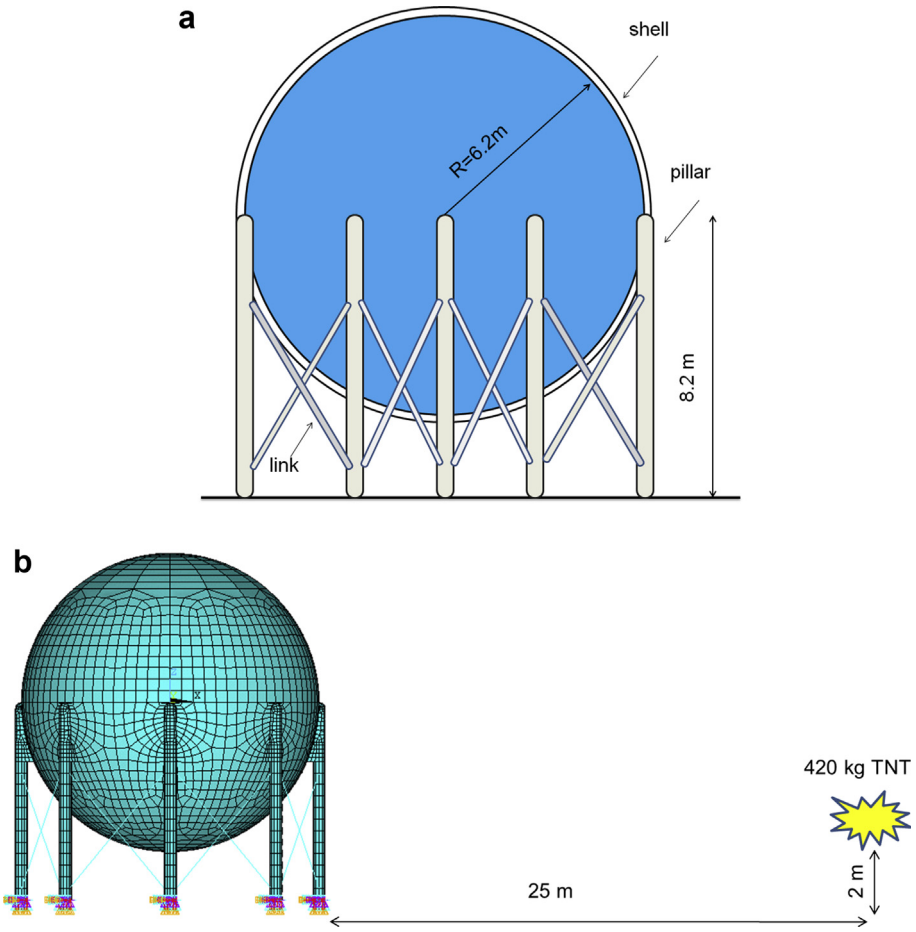

Fig. 1. Sketch of the spherical storage tank. (a) geometry and (b) finite element model.

where, σ_{dy} is the dynamic yielding strength considering strain rate effect, σ_y is the static yielding strength, ε^{pl} is the equivalent plastic strain rate, γ is the viscosity parameter, and m is the strain-rate hardening parameter. The suggested values of these two factors for steel are $\gamma = 60\ s^{-1}$ and $m = 4$ (Lu and Wang, 2012). The main mechanical parameters of the steel materials used in the structure are shown in Table 1.

Explosives have a density of 1630 kg/m^3, with an explosive speed of 6930 m/s and a C-J pressure of $2.1\,10^{10}$ Pa. The explosive charge was modeled using the high explosive burn material model and the Jones–Wilkin–Lee (JWL) equation of state (EOS). The JWL equation of state defines the pressure as a function of the relative volume, V and initial energy per volume, E, such that (Lee et al., 1973):

$$p = A\left(1 - \frac{\omega}{R_1 V}\right)e^{-R_1 V} + B\left(1 - \frac{\omega}{R_2 V}\right)e^{-R_2 V} + \frac{\omega E}{V} \tag{2}$$

Table 1
Parameters used in Cowper-Symonds model for steel material.

Tank part	Density (kg/m^3)	Young's modulus (N/m^2)	Poisson's ratio	Yield strength (MPa)	Failure strain
Sphere shell	7.8×10^3	2.06×10^{11}	0.3	305	0.20
Pillar	7.8×10^3	2.10×10^{11}	0.3	320	0.25
Junction	7.8×10^3	2.10×10^{11}	0.3	320	0.25
Link	7.8×10^3	2.10×10^{11}	0.3	225	0.25

where, E is the energy of explosion, and V is the relative volume of explosion. In the proposed model, the explosive equation of state parameters are defined as follows: $A = 3.74\,10^{11}$, $B = 3.23\,10^9$, $R_1 = 4.15$, $R_2 = 0.95$, $\omega = 7\,10^9$ and $E = 1$.

Air was modeled as an ideal gas and using the null material model and the pressure can be expressed using a linear polynomial EOS, which is a linear function of the internal energy per unit initial volume, E and is given by

$$P = C_0 + C_1\mu + C_2\mu^2 + C_3\mu^3 + \left(C_4 + C_5\mu + C_6\mu^2\right)E \tag{3}$$

where, $C_0 \sim C_6$ are user defined constants, E is the internal energy, μ is the parameter representing the characterization of fluid volume change and $\mu = \rho/\rho_0 - 1$, ρ_0 is the initial density of the air, and ρ is the current density of the air. The parameter values of the null material model and linear polynomial equation of state are shown in Table 2.

Water was modeled as compressible fluid with a Mie-Gruneisen equation of state, which uses a cubic shock velocity-particle velocity to define the pressure for compressed and stretched materials as (Stenberg, 1978; Gathers, 1994), in compression ($\mu > 0$)

Table 2
Parameters used in linear polynomial equation of state.

ρ_0 (kg/m^3)	E (Pa)	C_0	C_1	C_2	C_3	C_4	C_5	C_6
1.205	2.5×10^5	0	0	0	0	0.4	0.4	0

$$P = \frac{\rho_0 C_0^2 \mu \left[1 + \left(1 - \frac{\gamma_0}{2}\right)\mu - \frac{a}{2}\mu^2\right]}{\left[1 - (S_1 - 1)\mu - S_2 \frac{\mu^2}{1+\mu} - S_3 \frac{\mu^3}{(1+\mu)^2}\right]} + (\gamma_0 + a\mu)E \quad (4)$$

in tension ($\mu < 0$)

$$P = \rho_0 C_0^2 \mu + (\gamma_0 + a\mu)E \quad (5)$$

where $\mu = \rho_0/\rho - 1$, $\gamma_0 = 0.4934$ is the Gruneisen gamma, a is the first order volume correction to γ_0, ρ_0 is the density of water, E is the specific internal energy, C_0 is the sound speed at undisturbed state and S_1,S_2 and S_3 are constants (Cheng et al., 2005).

2.5. Estimation of the TNT equivalence of explosives

The blast effects of the vapor cloud explosion (VCE) are in the form of a shock wave composed of a high-pressure shock front, which expands outward from the center of the detonation, with the maximum overpressures decaying with distance (Jan, 2003). The TNT equivalent method has been widely used to estimate the explosive load of vapor clouds through an equivalent weight of a TNT-charge (Mannan, 2004; Planas-Cuchi et al., 2004). In order to estimate the maximum overpressure and the positive impulse at a specified distance, the chemical energy available in a vapor cloud is converted into an effective explosive weight of TNT on the basis of the following Equation (Baker et al., 1983):

$$W_{\mathrm{TNT}} = \alpha_e \frac{W_f Q_f}{Q_{\mathrm{TNT}}} \quad (6)$$

$$W_f = \rho V_e \xi \quad (7)$$

where, W_{TNT} is the equivalent mass of TNT that would produce the same effects as the explosion, α_e is an efficiency factor, it is generally accepted that, taking as a basis for calculation the total quantity of vapor in the cloud, the value of α_e is between 0.01 and 0.05 for most explosions (Lobato et al., 2006) (in this work, $\alpha_e = 0.03$), W_f is the total mass of hydrogen in the gas cloud, Q_f is the heat of combustion of hydrogen (0.418 MJ/kg), and Q_{TNT} is the heat of combustion of TNT (approximately 4.69 MJ/kg) (Van den Berg and Lannoy, 1993), ρ is the density of liquid hydrogen (approximately $0.5\,10^3$ kg/m^3) V_e is the volume of the liquid hydrogen inside the tank, ξ is an efficiency factor of the total amount of gasoline released (for the present work, $\xi = 0.35$), according to Equations (6) and (7), the equivalent mass of W_{TNT} was estimated at 420 kg.

2.6. Validation of blast model

The calculation results of the structural dynamic responses are highly dependent on the blast loading model. However, it is hard to obtain the accurate analytical solutions of the blast loading through simple analysis or hand calculation. With the development of computer techniques, numerical simulation has been an effective way to analyze and solve the problem of explosion, although the accuracy and the reliability of the calculated results need corresponding experimental verifications. Lu et al. (2011a, 2011b) conducted a series of explosion shock experimental studies on the dynamic response of floating-roof and fixed-roof tank specimens. The pressure characteristics caused by blast loading on the rigid wall of the large-scale anti-blast vessel was measured using high frequency dynamic pressure sensors. By using the shock wave pressure results obtained from the experiments (Lu et al., 2011a, 2011b), the accuracy and reliability of blast loading modeling techniques and the analysis procedures were validated. The ALE method and TNT equivalent method are employed to simulate the process of the combustible gas explosion, the propagation of air shock waves through the air, and the interaction of the explosion shock waves with the rigid wall of the large-scale anti-blast vessel. Fig. 2 shows the comparison of the simulation results and the experimental data (Lu et al., 2011a, 2011b). Fig. 2(a) and (b) show the pressure-time curves obtained from the different locations in the vessel with and without the clear reflected pressure wave. A detailed description of the modeling techniques and the validation can be found in Ref. (Lu et al., 2011a, 2011b). The validation study supports the accuracy and suitability of the proposed model to estimate the explosion loading.

3. Simulation results and discussions

3.1. Blast loading distribution

In order to measure pressure distribution of the explosive shock wave on the surface of the spherical storage tank structure, a number of measuring points are selected at difference locations on the spherical storage tank. Fig. 3 shows the details of the locations of these measuring points.

The pressure-time curves obtained from different measuring points are shown in Fig. 4. It reveals that the peak values for all of the points of the reflected pressure are higher than that of the incident ones. The maximum value is captured at point A, which is the spherical equator, with a value of 1.92 MPa as shown in Fig. 4(a). In comparison with the value of the pressure obtained at point A, the reflected pressures measured at point B and G are a little smaller, which are 1.67 MPa (Fig. 4(c)) and 1.45 MPa (Fig. 4(b)), respectively. It should be noted that the peak reflected pressure at

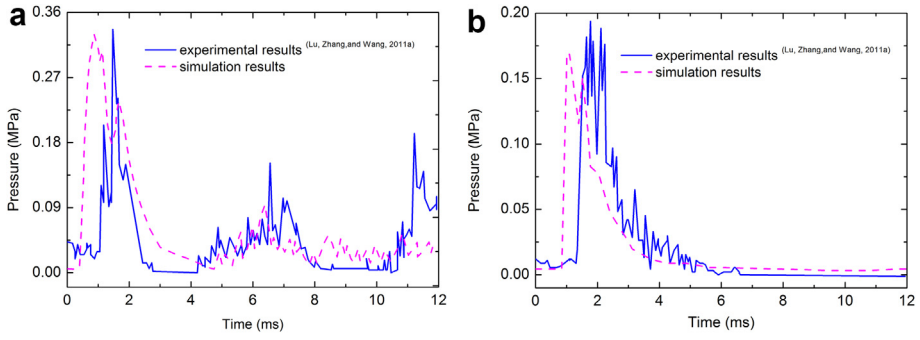

Fig. 2.

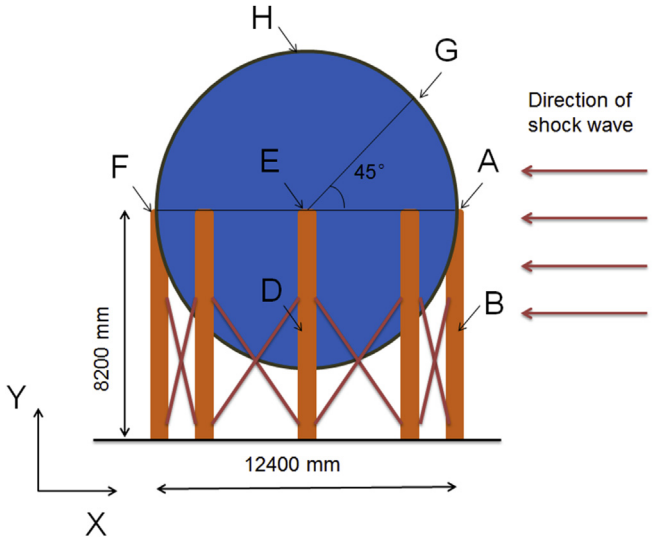

Fig. 3. Position of pressure test points on the spherical storage tank.

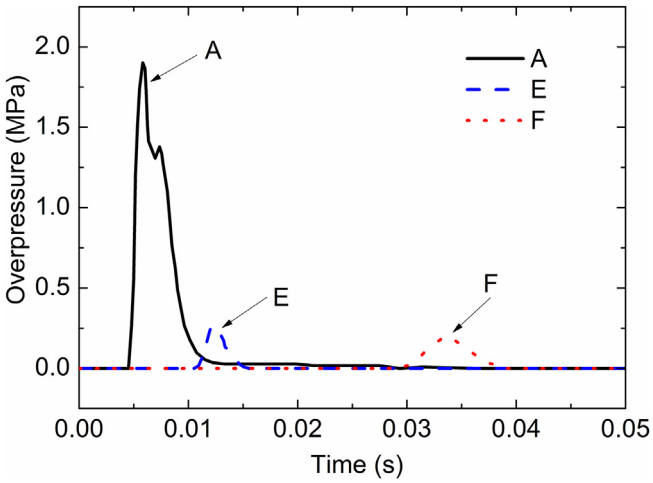

Fig. 5. Pressure-time curve in positions of point A, E and F.

point B (1.45 MPa), which is located on one of the pillars, is close to incident one (1.37 MPa), revealing that the pillars have only limited effects on the reflection of the shock wave. The measuring point, point H, from which the minimum peak pressure is captured, is located at the top of spherical storage tank. Almost the same values of reflected and incident pressure were observed at that point, which are 0.78 and 0.77 MPa (see in Fig. 4(d)), respectively.

The overpressure-time curves at point A, E and F are shown in Fig. 5. The entire diffraction process lasts about 30 ms. When the value of the overpressure obtained by point F, which is located at the back surface of the explosion, reaches its peak value, it indicates the end of the shock wave diffraction process. The peak overpressures at point A, E and F are 1.9 MPa, 0.27 MPa and 0.19 MPa, respectively, and the diffraction process moves forward with the shockwave. The value of the overpressure in the structure declined rapidly. The difference between the pressures at the front surface and back surface of the explosion induces horizontal displacement of the structure.

3.2. *Effective stress*

Time histories of the effective stress obtained at various points on the spherical storage tank are shown in Fig. 6. The effective stress plays an important role in determining structural damage and failure. High stress states are captured at point A and B, which are both located on the first row of the pillars along the direction of

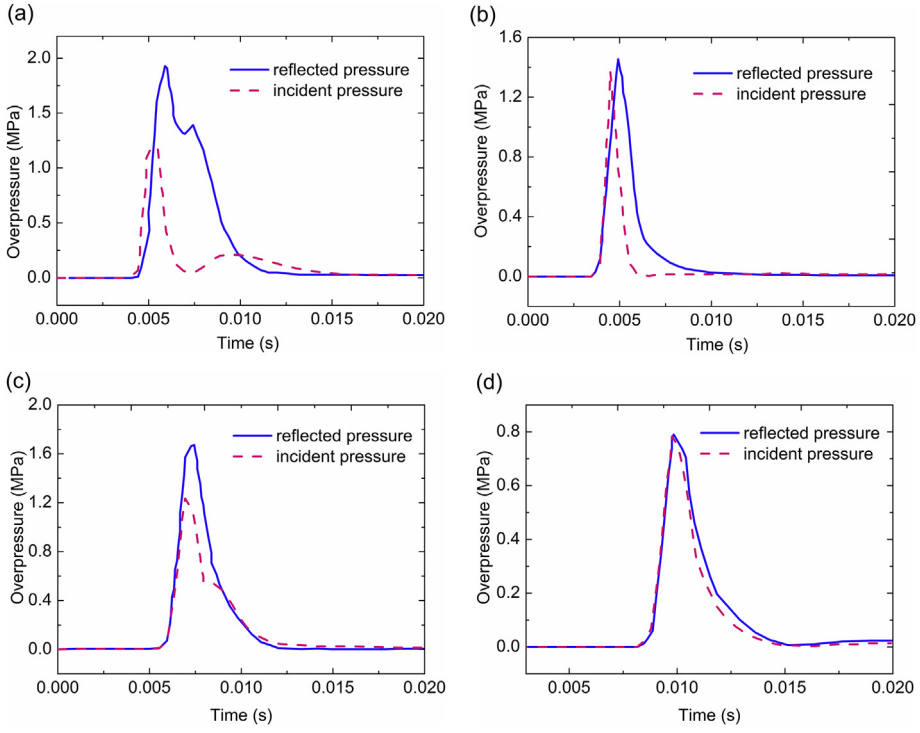

Fig. 4. Pressure-time curve of (a) point A, (b) point B, (c) point G and (d) point H.

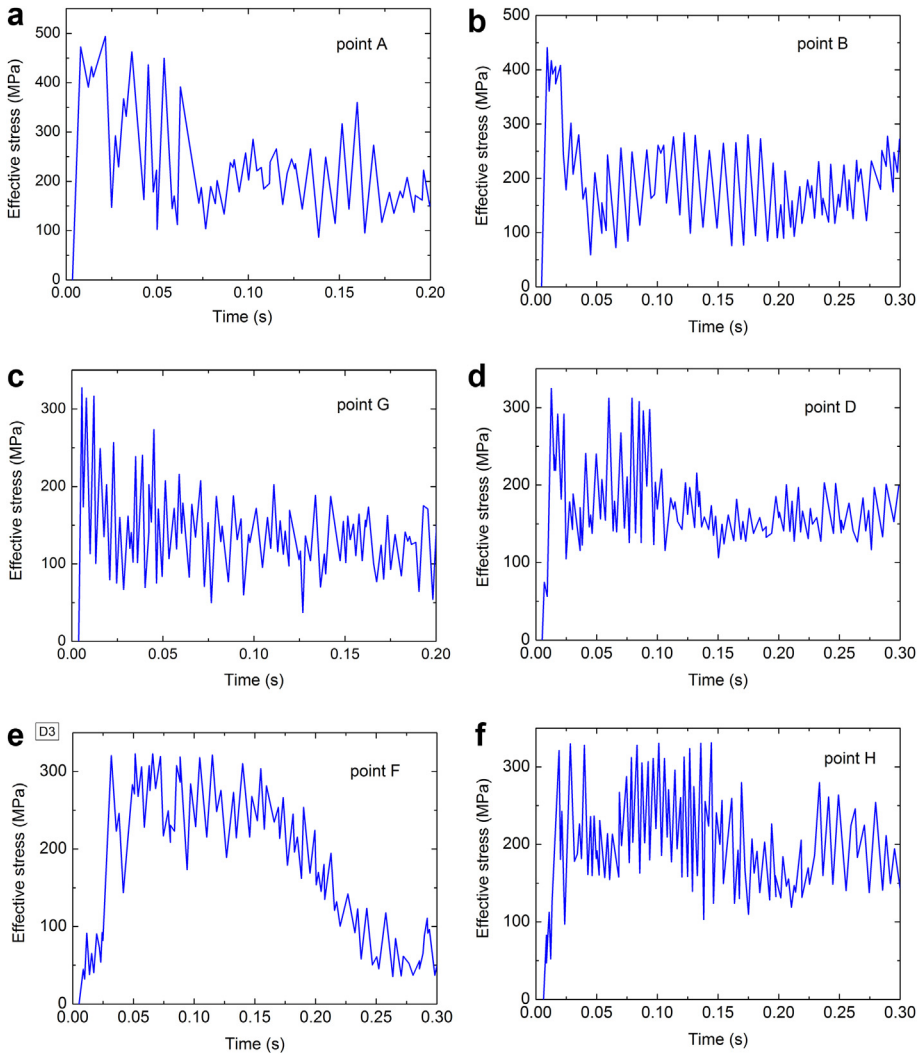

Fig. 6. Effective stress cloud charts for the spherical storage tank.

the shock wave. The maximum effective stress captured by all of these measuring points was captured by point A, which is located at the junction of the shell and a pillar. The peak effective stress at point A reaches 493 MPa at the moment of 0.002 s. The peak stress of point B reaches 440 MPa at the moment of 0.009 s. It is obvious that both of them have exceeded the yield strength of the steel.

3.3. Displacement response results

Fig. 7 shows the displacement–time curves of the spherical storage tank in the horizontal (X) and vertical (Y) direction under different TNT equivalence. The largest plastic deformation emerges in the first row of the pillars facing the explosion shock wave. Finite element analysis results show that the absolute value of displacement of the pillars reaches about 157 mm at the moment of 14.2 ms. According to Fig. 7(a), the displacement along the X direction changes with TNT equivalence. With the increase of TNT equivalence, residual deformation of the spherical shell also increases. However, changes in the values of the displacement with respect to various TNT equivalence along the Y direction are not evident. It can be seen from Fig. 7(b) that the vibration of the structure along the Y direction did not change as significantly with the increase of the TNT equivalence. Comparing the structural displacements in these two directions demonstrates that the maximum displacement of the tank in the X direction, is always much higher than the peak displacement along the Y direction. Therefore, when the TNT equivalence is high, the structure severely tilts along the direction of the impact. However, the lateral vibration caused by the impact is not so evident, which only has millimeter scale amplitude. Therefore, the lateral vibration has little effect on the dynamic responses of the spherical shell.

3.4. Failure analysis

Fig. 8 shows the representative failure process of the spherical storage tank under the explosion shock wave. When the shock wave reaches the surface of the spherical storage tank, the pillars located at the front surface of the explosion are subjected to a large stress with plastic deformation. At the initial stage of the failure process, the maximum effective stress was observed at the connection of the pillar and the shell due to the effects of the stress concentration, which has a magnitude of 1358 MPa at 9.9 ms (Fig. 8(a)). Then significant deformation occurred at the first row of the pillars facing the explosion at 14.2 ms (Fig. 8(b)). During the shock wave propagation, significant bending deformation and shear breakage were observed in the pillars facing the explosion,

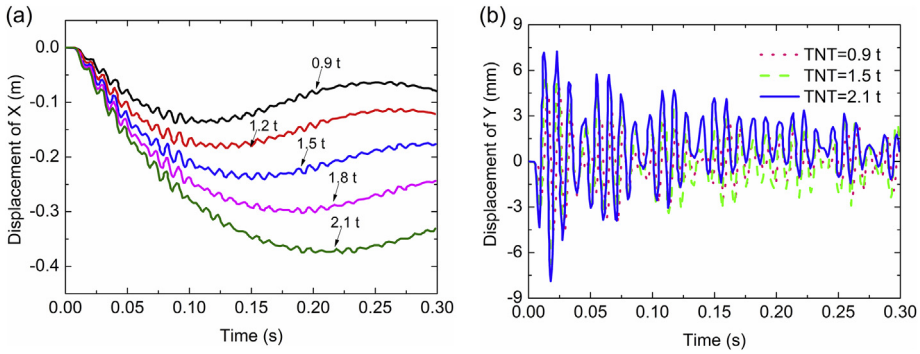

Fig. 7. Displacement of (a) X and (b) Y.

and concaved buckling of the spherical shell was also found at the moment of 20.9 ms (Fig. 8(c)). The final failure mode shows that global damage of the structure occurs. At the moment of 40.4 ms, some of the pillars lost the support for the spherical shell under the blast loads. A significant amount of concaved deformation was observed at the surface of the spherical shell and some holes can be found on the surface of the spherical storage tanks (Fig. 8(d)).

3.5. Energy distribution in the tank

After the shock wave is applied to the spherical storage tank structure, each part of the structure gains initial energy, which is comprised of two forms of energy transformation. One is the conversion between the internal energy and kinetic energy of the structure, and another is the transfer of energy between the structural members of the tanks themselves. In this study, the analysis did not consider the damping effect of the structure and did not consider the energy dissipation.

Fig. 9(a) shows the changes of total energy of the whole tank under the gas explosion with time. The total energy of the tank reached a relatively stable value (approximately 13 MJ) at the moment of 20 ms after the explosion. Fig. 9(b) shows that most of the energy of the tank is the internal energy, which manifests as the strain energy stored in the pillars, and is caused by the bending deformation of the pillars at the front surface of the explosion after the blast wave. Another part of energy is kinetic energy since the tank moves at a constant velocity. When the speed is reduced to 0, the maximum displacement value occurs along the direction of the shock wave. Since large plastic deformation of the pillars occurs, which act as the control member of the stiffness of the structure, the shape or the position of the tank can not return to its initial state. Then, the kinetic energy is gradually converted into internal energy, manifesting as the tensile or compressive deformation of all the pillars caused by the movement of the upper structure. It can be

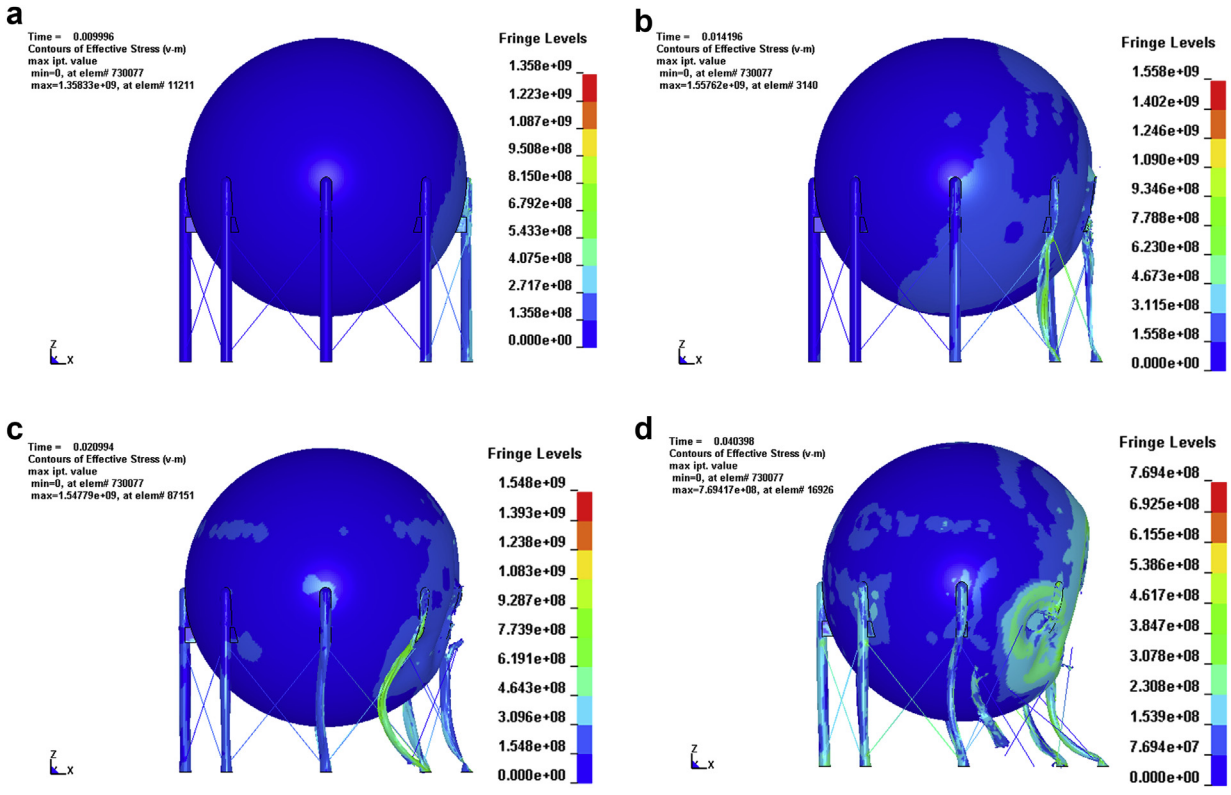

Fig. 8.

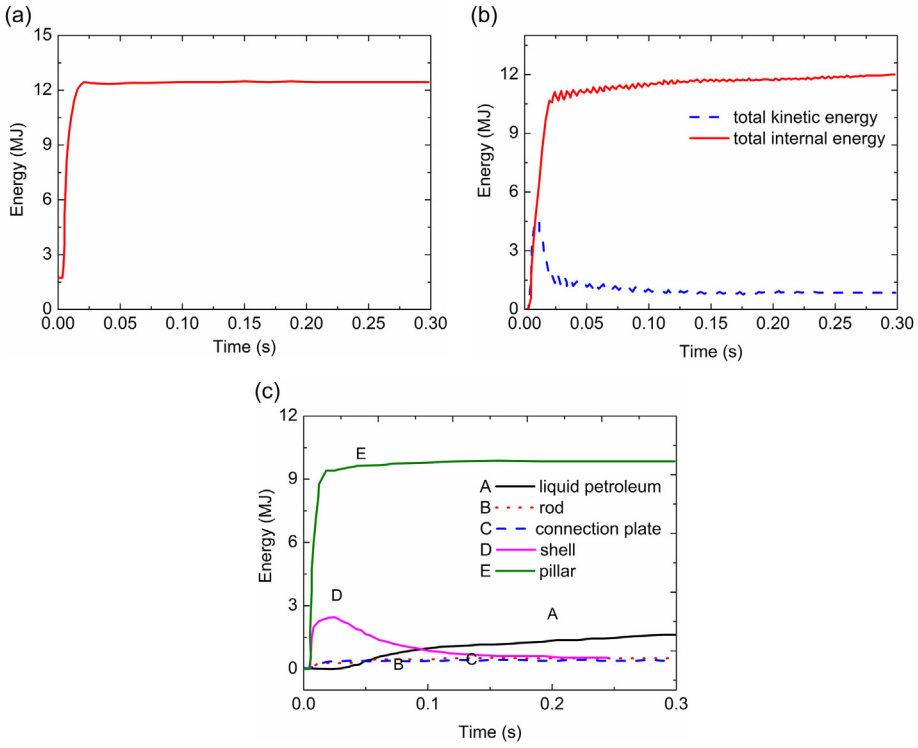

Fig. 9. Energy time curve of (a) total energy, (b) total inner energy and kinetic energy, and (c) various parts of the tank energy.

seen that the initial internal energy obtained by the tank is the key factor which leads to the large deformation and destruction. However, the initial kinetic energy is the major influencing factor of displacement. Fig. 9(c) shows the energy–time curve of each part of the tank, and it is clear that the internal energy of the pillars is higher than that of other parts of the structure.

3.6. *Influence of liquid level in the tank*

The displacement and energy values with different liquid levels in the spherical storage tank under blast loading are listed in Table 3. When calculating the energy, the energy of the contained liquefied petroleum gas in the tank is not considered. Thus, the tabulated energy can be used to represent the energy of the tank itself in an accurate manner. As shown in Table 3, the increase of the liquid level in the tank may cause a great influence on the dynamic response of the structure in the *X* direction but has little effect in the *Y* direction. As the liquid level increases from 0 to 80%, the displacement of the structure in the *X* direction is reduced by 59.1%, and the internal energy is reduced by 7.4%. The reason is that the fluid in the spherical storage tank lead to increasing of damping of the structure, thus part of energy induced by the impact of the blast was absorbed. Therefore, the dynamic response the spherical storage tanks could be decreased with the increasing of the fluid inside the tank under blast loading.

Table 3
Influence of liquid level in the spherical tank.

Liquid level (%)	Displacement of *X* (mm)	Displacement of *Y* (mm)	Total energy (MJ)	Internal energy (MJ)
0	384	6.87	11.895	11.686
50	241	6.88	11.261	11.188
80	157	6.88	10.903	10.816

4. Conclusions

A numerical study of the dynamic responses and failure process of spherical storage tanks subjected to combustible gas explosions is conducted by using the explicit nonlinear dynamic finite element program LS-DYNA. The TNT equivalent method is used in this study. The following conclusions can be drawn:

- The spherical tank has significant effects on the reflection of the shock waves under blast loading, which decrease from the equator to the poles of the sphere. However, the pillars can only reflect a limited amount of the shock waves.
- The damages caused by the blast to the spherical tank include: (1) significant bending deformation of the pillar; (2) local sag of the spherical shell; and (3) fracture in the connections between the pillars and the spherical shell. Since significant stress concentration under blast loading is generated at the connections between the pillars and the spherical shell, the supporting system plays an important role in controlling the structural damages to the spherical tank.
- The initial internal energy obtained by the spherical tank from the explosion is a key factor leading to extensive damages and large deformation of the structure. On the other hand, the displacement of the tank is related to the initial kinetic energy. Since the liquid stored in the tank can absorb energy from the impact of the explosion, the responses of the spherical tank can be reduced at an early stage after the impact.

Acknowledgments

The authors thank the financial support of the National Natural Science Foundation of China (Grant No. 51108141) and the Natural Science Foundation of Heilongjiang Province of China (Grant No. QC2011C064).

References

Abbasi, T., Abbasi, S.A., 2007. The boiling liquid expanding vapour explosion (BLEVE): mechanism, consequence assessment, management. J. Hazard Mater. 141 (3), 489–519.

Baker, W.E., Cox, P.A., Westine, P.S., Kulesz, J.J., Strehlow, R.A., 1983. Explosion Hazards and Evaluation, Fundamental Studies in Engineering. Elsevier Scientific Publishing Company, Amsterdam.

Chang, J.I., Lin, C.C., 2006. A study of storage tank accidents. J. Loss Prev. Process Ind. 19 (1), 51–59.

Chen, M., Hung, K.C., Chong, O.Y., 2005. Numerical study of water mitigation effects on blast wave. Shock Waves 14 (3), 217–223.

Cowper, G.R., Symonds, P.S., 1957. Strain-hardening and Strain-rate Effects in the Impact Loading of Cantilever Beams (No. TR C 11 28). Brown Univ Providence Ri.

Dogangun, A., Karaca, Z., Durmus, A., Sezen, H., 2009. Cause of damage and failures in silo structures. J. Perform. Constr. Facil. 23 (2), 65–71.

Drosos, J.C., Tsinopoulos, S.V., Karabalis, D.L., 2005. Seismic response of spherical liquid storage tanks with a dissipative bracing system. In: 5th GRACM International Congress on Computational Mechanics, Limassol, vol. 29, pp. 313–319.

Evans, D.V., Linton, C.M., 1993. Sloshing frequencies. Q. J. Mech. Appl. Math. 46 (1), 71–87.

Gathers, G.R., 1994. Shock Wave Physics and Equation of State Modelling. World Scientific Publishing Co. Pte. Ltd, Singapore.

James, R.W., Raba, G.W., 1991. Behavior of welded steel water-storage tank. J. Struct. Eng. 117 (1), 61–79.

Jan, S., 2003. Experimental evaluation of LPG tank explosion hazards. J. Hazard Mater. 96 (2–3), 189–200.

Karamanos, S.A., Patkas, L.A., Platyrrachos, M.A., 2006. Sloshing effects on the seismic design of horizontal-cylindrical and spherical industrial vessels. J. Press. Vessel Technol. 128 (3), 328–340.

Kim, J.S., An, D.H., Lee, S.Y., Lee, B.Y., 2009. A failure analysis of fillet joint cracking in an oil storage tank. J. Loss Prev. Process Ind. 22 (6), 845–849.

Korkmaz, K.A., Sari, A., Carhoglu, A.I., 2011. Seismic risk assessment of storage tanks in Turkish industrial facilities. J. Loss Prev. Process Ind. 24 (4), 314–320.

Lee, E., Finger, M., Collins, W., 1973. JWL Equation of State Coefficients for High Explosives (No. UCID–16189).

Lees, F.P., 1996. Loss Prevention in the Process Industries: Hazard Identification, Assessment and Control. Butterworth-Heinemann.

Lieb, J.M., 2002. Recent developments in API storage tank standards to improve spill prevention and leak detection/prevention. In: Proceedings of the US EPA Fourth Biennial Freshwater Spills.

Lobato, J., Canizares, P., Rodrigo, M.A., Saez, C., Linares, J.J., 2006. A comparison of hydrogen cloud explosion models and the study of the vulnerability of the damage caused by an explosion of H2. Int. J. Hydrog. Energy 31 (12), 1780–1790.

LSTC, 2007. LS-DYNA Keyword User's Manual Version 971. Livermore Software Technology Corporation.

Lu, S.Z., Wang, W., 2012. Study of destruction mechanism of floating-roof oiltank under combustible gaseous explosion in a small scale experiment. Appl. Mech. Mater. 137, 65–71.

Lu, S.Z., Wang, W., Zhang, B.Y., 2011a. Experimental research on destruction mechanism of large-scale floating-roof oil tank under blast loading. Explos. Shock Waves 2, 158–164 (in Chinese).

Lu, S.Z., Zhang, B.Y., Wang, W., Zhang, C.W., 2011b. Experimental research on dynamic response mechanism of thin cylindrical shell under blast loading. J. Nanjing Univ. Sci. Technol. 5, 621–626 (in Chinese).

Mannan, S. (Ed.), 2004. Lees' Loss Prevention in the Process Industries: Hazard Identification, Assessment and Control. Butterworth-Heinemann.

McIver, P., 1989. Sloshing frequencies for cylindrical and spherical containers filled to an arbitrary depth. J. Fluid Mech. 201, 243–257.

McIver, P., McIver, M., 1993. Sloshing frequencies of longitudinal modes for a liquid contained in a trough. J. Fluid Mech. 252, 525–541.

Moslemi, M., Kianoush, M.R., 2012. Parametric study on dynamic behavior of cylindrical ground-supported tanks. Eng. Struct. 42, 214–230.

Patkas, L.A., Karamanos, S.A., 2007. Variational solutions for externally induced sloshing in horizontal-cylindrical and spherical vessels. J. Eng. Mech. 133 (6), 641–655.

Persson, H., Lönnermark, A., 2004. Tank Fires. SP Report, 14.

Planas-Cuchi, E., Salla, J.M., Casal, J., 2004. Calculating overpressure from BLEVE explosions. J. Loss Prev. Process Ind. 17 (6), 431–436.

Sezen, H., Livaoglu, R., Dogangun, A., 2008. Dynamic analysis and seismic performance evaluation of above-ground liquid-containing tanks. Eng. Struct. 30 (3), 794–803.

Shebeko, YuN., Bolodian, I.A., Molchanov, V.P., Deshevih, YuI., Gordienko, D.M., Smolin, I.M., Kirillov, D.S., 2007. Fire and explosion risk assessment for large-scale oil export terminal. J. Loss Prev. Process Ind. 20, 651–658.

Stenberg, D.J., 1978. Spherical Explosions and the Equation of State of Water, UCID-2097. USA. Lawrence Livermore National Laboratory, Livermore, CA.

Trebuňa, F., Šimčák, F., Bocko, J., 2009. Failure analysis of storage tank. Eng. Fail. Anal. 16 (1), 26–38.

Van den Berg, A.C., Lannoy, A., 1993. Methods for vapour cloud explosion blast modelling. J. Hazard Mater. 34, 151–171.

Zhou, J.W., Fang, Q., Zhang, Y.D., 2009. Numerical analysis of fluid-solid coupling of the underground liquid-storage tanks subjected to the ground shock induced by explosions. J. Disaster Prev. Mitig. Eng. 1, 35–43 (in Chinese).